Real-Time Capacitive Sensor Applied to a Train Wagon Prototype for Measuring Iron Ore Moisture

Gabriel A. Santos ⓘ , Érica S. Pinto ⓘ , Artur J. C. da Silva ⓘ , Paulo M. de B. Monteiro ⓘ , André L. A. Mesquita ⓘ , and Alan Kardek R. Segundo ⓘ

Abstract—The emission of particulates during rail transport is related to the low moisture of the ore, which causes environmental pollution along the railroad. Given this problem, this work proposes the development of a parallel plate capacitive sensor applied to a small wagon prototype made of acrylic to measure the iron ore moisture and support studies of particulate emissions carried out in a laboratory. The sensor uses the Real-Dual Frequency method, which decreases the influence of electrical conductivity on the dielectric constant, even using low frequency (up to 8 MHz). From the dielectric constant, iron ore moisture is determined from indirect calibration, which obtained an accuracy of 0.07 pp and a maximum error of 0.39 pp. This study shows the development of an innovative real-time capacitive sensor, which uses a modern impedance-based technique to investigate particulate emissions and the drying behavior of iron ore.

Index Terms—Capacitive sensor, Moisture, Iron ore, Train wagon, Dielectric constant.

I. INTRODUCTION

Mining is of great importance to the Brazilian economy. In 2021, for example, 70% of its trade balance came from this sector, and iron ore represented 76% of the revenue [1]. Although mining has great economic value, it also has a tremendous environmental impact.

The problem related to rail transport by train wagons is the loss of mass caused by wind drag in the surface layer of the ore. The particulate emitted causes environmental pollution around the railroad. According to [2, 3], adding water to the surface layer of the ore in the train wagon is a quick solution to avoid particulate emissions, as the interstitial water in the ore generates a capillary force that opposes the shear force generated by wind drag. However, studying dust generation or particulate emission in train wagons is hazardous due to operational, repetitive, and safety conditions [2].

To comprehend the drying behavior and particulate emission of iron ore in rail transportation in safe conditions, some researchers have been using wind tunnels, like dos Santos Jr

Gabriel Almeida Santos and Paulo Marcos de Barros Monteiro are with the Programa de Pós-Graduação em Instrumentação, Controle e Automação de Processos de Mineração, Universidade Federal de Ouro Preto, and also with the Instituto Tecnológico Vale, Ouro Preto 35400-000, Brazil (e-mail: gabrielalmeida.el@gmail.com; pmemop@gmail.com).

Érica Silva Pinto and Alan Kardek Rêgo Segundo are with the Programa de Pós-Graduação em Instrumentação, Controle e Automação de Processos de Mineração and a Programa de Pós-Graduação em Ciência da Computação, Universidade Federal de Ouro Preto, and also with the Instituto Tecnológico Vale, Ouro Preto 35400-000, Brazil (e-mail: erica.pinto@ufop.aluno.edu.br; alankardek@ufop.edu.br).

Artur J. C. da Silva and André L. A. Mesquita are with Universidade Federal do Pará, Tucuruí 68455-901, Brazil (e-mail: arturjose@ufpa.br; andream@ufpa.br).

et al. [4], that simulate airflow in small-scale train wagon prototypes. However, there is no technology to assist this application in the ore real-time moisture measurement, which traditionally uses the gravimetric method. Although this technique is the most direct and accurate, it is sample destructive and has a very long response time, about 4 hours at 105 ℃ [5].

Moisture measurement along the mining production chain is also necessary to control the amount of water in the final product. In addition to the high production cost, increased moisture can bring problems such as low stability of stockpiles and transport risks, mainly related to maritime transport. The long response time of the gravimetric method does not always favor efficient decision-making [6, 7].

In recent years, dielectric sensors have been widely used for the non-destructive and real-time determination of soil moisture. It uses the difference between the apparent dielectric constant (ε) of dry soil (about 2-5) and pure water (about 80) to estimate soil moisture [8]. Despite the fast response time, the sensor's output signal also is prone to errors from soil texture (dimension and size of particles), electrical conductivity (σ), and temperature.

In the iron ore case, some researchers have developed similar sensors used with soils, aiming for real-time monitoring. Lage et al. [9] proposed the development of a capacitive sensor to be used in the test bench that correlates the moisture with ε, and also relates dependence from iron content and density. Silva et al. [10] proposed a non-invasive and coplanar capacitive transducer for the online determination of iron ore moisture in silos. Segundo et al. [11, 12] proposed the development of a cylindrical capacitive sensor based on a current-voltage (I-V) converter circuit to measure soil impedance. Pinto et al. [7, 13] proposed the development of a capacitive sensor with 2 degrees of freedom on a laboratory scale to measure the iron ore moisture in a conveyor belt. Those contributions overcame accuracy problems related to contactless methods like infrared and microwave analyzers [7].

Thus, to contribute to the particulate emission problem, this work proposes the development of a capacitive moisture sensor for real-time measurement applied to a train wagon prototype built on a small scale only for laboratory use. The importance of addressing this issue is providing a sensor specially designed to investigate the drying behavior of iron ore in dust studies in wind tunnels.

II. METHODOLOGY

The prototype of the wagon used in this work was developed based on the specifications of the wagon that transports ore on the Estrada de Ferro Vitória a Minas (EFVM), Brazil, by one of the largest mining companies in the world, Vale SA. We carried out the wagon and the measurement system development in the Multiuser Automation Laboratory of UFOP, and the execution of the drying test was performed in the wind tunnel of the Fluid Dynamics and Particulates Laboratory of UFPA.

A. Capacitive Sensor

Earlier tests at the Fluid Dynamics and Particulates Laboratory of UFPA used a train wagon prototype, in a reduced 1x20 scale, of the wagon series 218000-6 to 219159-8 used in the EFVM, as shown in Fig. 1
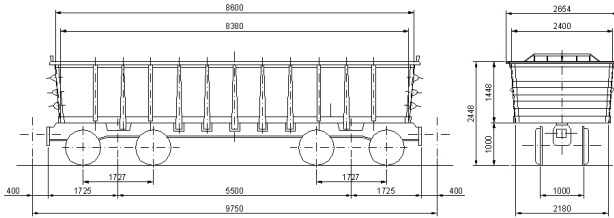
Fig. 1. Train wagon series 18000-6 to 219159-8 used in EFVM. Total length of 8600 mm, width of 2440 mm, and height of 1448 mm [14].

As the previous prototype had a rectangular shape, we designed a new prototype with a parallel plate capacitive sensor. Thus, the sides of the prototype configure the sensor electrodes, and the iron ore configures the dielectric medium. We made the base of 6 mm acrylic and 1x20 scale, and the sensor was composed of 1 mm stainless steel plates with a length L equal to 429.5 mm and a height H equal to 57.4 mm. The distance d between the plates is 120 mm, as shown in Fig. 2.
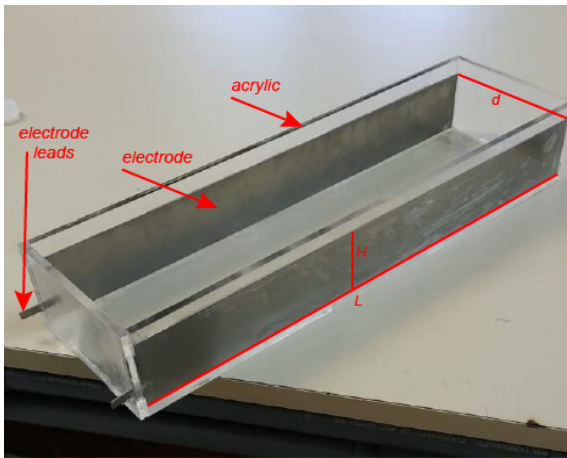
Fig. 2. Capacitive sensor applied to a train wagon prototype. Total length of 429.5 mm, height of 57.4 mm, and distance of 120 mm.

The admittance $\mathbf{Y}$ of a capacitor is expressed by:

$$\mathbf{Y} = j\omega k_g \varepsilon_o \boldsymbol{\varepsilon_r} \tag{1}$$

where $j = \sqrt{-1}$, ω is the angular frequency ($rad \cdot s^{-1}$), k_g is the sensor geometric constant (= 0,204 m), $\varepsilon_o = 8.854 \ pF \cdot m^{-1}$ is the vacuum dielectric constant and $\boldsymbol{\varepsilon_r}$ is the complex permittivity.

The complex permittivity describes the interaction of a material with an external electric field. The circuit developed for this work uses excitation frequencies of 500 kHz and 8 MHz then, according to [15, 16], the complex permittivity can be expressed by its low-frequency equivalent, as shown in Eq. (2).

$$\boldsymbol{\varepsilon_r} = \varepsilon - j\frac{\sigma}{\omega\varepsilon_0} \tag{2}$$

where ε is the dielectric constant and σ is the electrical conductivity.

By replacing Eq. (2) in Eq. (1), the admittance of a capacitor can be represented as:

$$\mathbf{Y} = k_g(\sigma + j\omega\varepsilon_0\varepsilon) \tag{3}$$

Thus, for the sensor developed with parallel plates, Fig. 2, the conductance G is a function of the electrical conductivity σ, and the capacitance C is a function of the dielectric constant ε, respectively shown in Eq. (4) and Eq. (5).

$$G = K_g\sigma \tag{4}$$

$$C = k_g\varepsilon_0\varepsilon \tag{5}$$

B. Real-Dual-Frequency

Reference [19] presented a method for calculating impedance using an I-V converter with a trans-impedance amplifier. The circuit gains for the two excitation frequencies, $f_0 = 500$ kHz and $f_1 = 8$ MHz, are directly related to the dielectric constant and electrical conductivity of the medium. However, in this case, the conductivity of the medium under test can influence the measurement of the dielectric constant.

In the method Real-Dual-Frequency developed by [11], the system gains A_0 and A_1 are used to calculate the impedance of the medium. Eq. (6) and Eq. (7) show the A_0 and A_1 gains, respectively.

$$A_0 = \sqrt{\frac{G_x^2 + \omega_0^2 C_x^2}{G_f^2 + \omega_0^2 C_f^2}} \tag{6}$$

$$A_1 = \sqrt{\frac{G_x^2 + \omega_1^2 C_x^2}{G_f^2 + \omega_1^2 C_f^2}} \tag{7}$$

where G_x and C_x are the conductance and capacitance of the unknown medium, respectively; G_f and C_f are the conductance and capacitance of the reference impedance of the circuit, respectively, and ω_0 and ω_1 are the angular frequencies of the excitation frequencies, respectively. The system cut-off frequencies $f_{zf} = \frac{1}{2\pi R_f C_f}$ and $f_{zx} = \frac{1}{2\pi R_x C_x}$ depend on the circuit reference impedance and the impedance of the unknown medium, respectively.

Since G_f, C_f, ω_0 and ω_1 are known, and the sensor measures A_0 and A_1, the conductivity σ and dielectric constant ε of the medium can be found by isolating G_x and C_x from Eq. (6)

and Eq. (7), and replacing them in Eq. (4) and Eq. (5). Then, σ and ε from the unknown medium can be expressed as:

$$\sigma = \frac{1}{k_g} \sqrt{\frac{A_1^2 \omega_0^2 (G_f^2 + \omega_1^2 C_f^2) - A_0^2 \omega_1^2 (G_f^2 + \omega_0^2 C_f^2)}{\omega_0^2 - \omega_1^2}} \quad (8)$$

$$\varepsilon = \frac{1}{\varepsilon_0 k_g} \sqrt{\frac{A_0^2 (G_f^2 + \omega_0^2 C_f^2) - A_1^2 (G_f^2 + \omega_1^2 C_f^2)}{\omega_0^2 - \omega_1^2}} \quad (9)$$

This method independently calculates the values of σ and ε, even when the excitation frequencies are at the threshold of the cutoff frequencies of the system, that is, in the decay region of 20 dB/dec.

The electronic measurement circuit used in this work has a 8-bit PIC18F25K80 microcontroller for signal generating and data-processing, and more details are presented by [11].

C. σ and ε Calibration

Reference samples with known σ and ε, such as distilled water, alcohol, and combinations of $H2O$ and $NaCl$ solutions, were used in the calibration process. The reference values for ε were taken from the literature [7], while reference values for σ were measured by the Del Lab DL-150P conductivity meter. Table I shows the reference samples.

TABLE I
REFERENCE SAMPLES FOR σ AND ε.

Sample	σ $(\mu S/cm)$	ε
Distilled water	14.48	80.2
Potable water	30.65	80.2
Concentration 1 ($H_2O + NaCl$)	123.80	80.2
Concentration 2 ($H_2O + NaCl$)	257.90	80.2
Concentration 3 ($H_2O + NaCl$)	426.20	80.2
Concentration 4 ($H_2O + NaCl$)	864.40	80.2
Alcohol 25% + H2O 75%	5.44	69.6
Alcohol 50% + H2O 50%	6.95	54
Alcohol 75% + H2O 25%	6.84	39.3
Alcohol	6.06	25.2
Air	0	1

Through reference samples, we calculated the Reference Gains with Eq. (6) and Eq. (7). Then, with the Measured Gains, measured by the sensor, we plotted the curve Measured Gains vs. Reference Gains to generate the model that corrects the gains of the sensor.

After that, we measured σ and ε with the Real-Dual-Frequency method through Eq. (8) and Eq. (9), and an adjustment of σ and ε was carried out with the Reference σ and ε to obtain the correction models.

Fig. 3 and Fig. 4 show σ and ε Measured, respectively, after applying the correction model. The method obtained a linear tendency between the Reference and Measured values for the Reference samples.
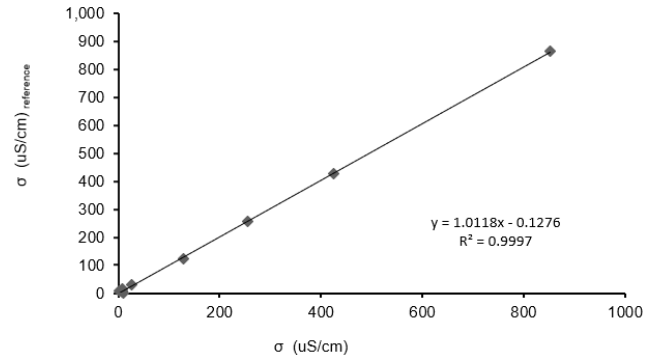
Fig. 3. Measured σ vs. Reference σ.
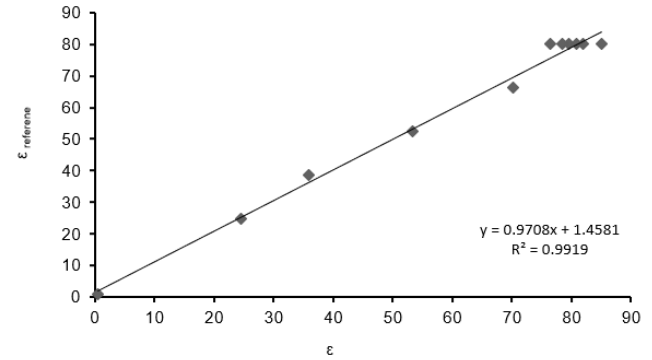
Fig. 4. Measured ε vs. Reference ε.

The calibration was performed to mediums with conductivity up to 864.4 µS/cm. The ε measurements for water samples concentrated around 80, like the references.

D. Moisture Calibration

Chen and Chen [17] performed an experiment to determine the optimum number of points to calibrate a capacitive sensor and showed that 5 points of saturated salt solutions are the best number, however, 5, 7, and 11 points are also suitable for industrial applications. Robinson et al. [18] and Topp and J. L. Davis and [19] showed that for a wide range of mineral soils third-order polynomial regressions are the best way to demonstrate the strong dependence between moisture and ε.

For the moisture calibration process, we prepared, on a wet basis, seven compacted iron ore samples between 0% and 13%. The samples presented in Table II, encompass the range of commercial interest (7%-9%).

TABLE II
MOISTURE SAMPLES FOR CALIBRATION.

Sample	Moisture (%)
1	0.69
2	1.48
3	3.70
4	5.91
5	8.09
6	10.35
7	12.90

The composition of iron ore tested was 66.86% Fe (Iron), 2.63% SiO2 (Silica), and the rest are non-significant compositions. Fig. 5 presents the iron ore inserted in the prototype.

Fig. 5. Iron ore inserted in the prototype.

First, we took ten measurements with the sensor for each sample and calculated the average gain. After that, we obtained σ and ε with Real-Dual-Frequency method and corrected them with the models generated in the σ and ε calibration process. Finally, we obtained the moisture model by plotting the ε vs. Moisture curve, as shown in Fig. 6.
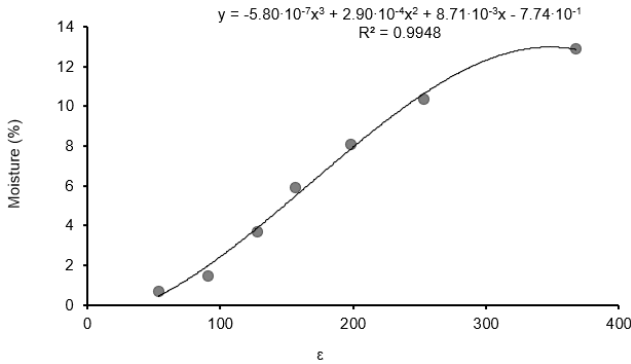
Fig. 6. Iron ore moisture model.

The moisture calibration model has a third-order polynomial regression with a determination coefficient R^2 equal to 0.9948. The dielectric constant ε for the 12.9% sample was 367.24, and the conductivity σ was 786.61 $\mu S/cm$.

To verify the moisture calibration error, we performed a statistical analysis. We took ten measurements for each sample and then obtained the average moisture. Fig. 7 presents the error curve where b is the bias of the measurement and U is equal to the measurement uncertainty ($U = t \cdot u$), obtained with the Student's t distribution and the standard uncertainty of the mean u.
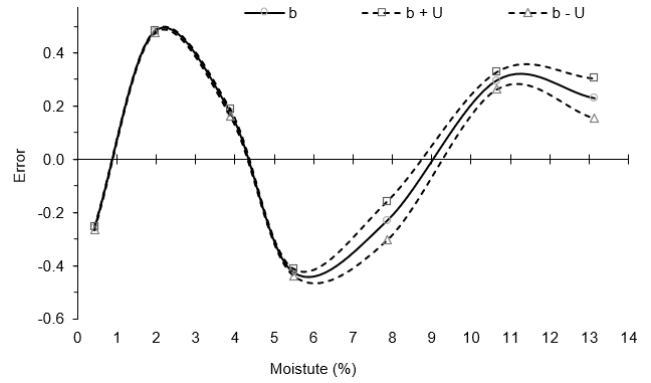
Fig. 7. Error curve for the moisture calibration.

The calibration obtained a small measurement uncertainty U, demonstrating the quality of the measurement. The maximum measurement uncertainty was 0.08 %, and the maximum error was 0.48 pp (percentage point) for the 1.48 % moisture sample.

Aiming to validate the calibration model obtained in Fig. 6, we prepared more samples within the moisture range calibration, as shown in Table III.

TABLE III
VALIDATION MOISTURE SAMPLES.

Sample	Moisture (%)
1	1.47
2	2.68
3	4.39
4	5.80
5	7.90
6	10.11
7	11.720

In the validation process, was taken only one measurement for each moisture sample. Table IV presents the results, where CQV corresponds to the conventional quantity value of moisture taken by the gravimetric method, I corresponds to the measurement indication, C corresponds to the correction of the bias taken by linear interpolation regions of the Fig. 7, MR corresponds to the measurement result ($MR = I + C$), U corresponds to the measurement uncertainty from the calibration process, and the $Error$ corresponds to $MR - CQV$.

TABLE IV
VALIDATION RESULTS OF IRON ORE MOISTURE
MEASUREMENTS..

CQV (%)	I (%)	C (pp)	MR ± U (%)	Error (pp)
1.47 ± 0.01	1.67	-0.34	1.33 ± 0.01	-0.14
2.68 ± 0.01	2.96	-0.32	2.64 ± 0.01	-0.03
4.39 ± 0.01	4.44	-0.03	4.47 ± 0.01	0.08
5.8 ± 0.01	5.44	0.41	5.84 ± 0.01	0.05
7.9 ± 0.01	8.11	0.18	8.29 ± 0.07	0.39
10.11 ± 0.01	10.56	-0.28	10.28 ± 0.03	0.16
11.72 ± 0.01	11.80	-0.27	11.53 ± 0.03	-0.19

The sensor presented an uncertainty of 0.07 pp and a maximum moisture error of 0.39 pp for the most commercial interest region (7%-9%). For other moistures range, the error was less than 0.19 pp.

E. Wind Tunnel

Aiming to understand the drying behavior of iron ore, [20] carried out a study to characterize the drying behavior of pellet feed and sinter feed iron ores under a speed of 1 m/s and temperatures of 50 °C, 60 °C, 70 °C, and 80 °C. dos Santos Jr et al. [4] developed a subsonic wind tunnel with an open circuit blower and closed test section to be used in particulate emission studies. In this type of wind tunnel, the air is blown by the fan at the end of the tunnel, the test section is closed and the air is released to the environment through the opening of the circuit at the other end, Fig. 8.
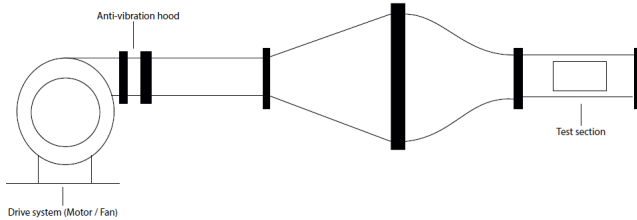
Fig. 8. Open circuit fan wind tunnel model.

The moisture sensor developed in this project was applied in the wind tunnel test section to assist in the study of the drying behavior of iron ore in real-time.

III. RESULTS AND DISCUSSION

The iron ore used in the UFPA Laboratory is of the Pellet Feed type. So, after proving the sensor accuracy in the UFOP Laboratory, it was necessary to perform a new moisture calibration for the iron ore used in the UFPA Laboratory.

Fig. 9 presents the moisture calibration for the pellet feed. The curve obtained was from the third order with $R^2 = 0.9805$.

$$y = 2.57 \cdot 10^{-3} x^3 - 1.03 \cdot 10^{-1} x^2 + 1.50x - 7.94 \cdot 10^{-1}$$
$$R^2 = 0.9805$$
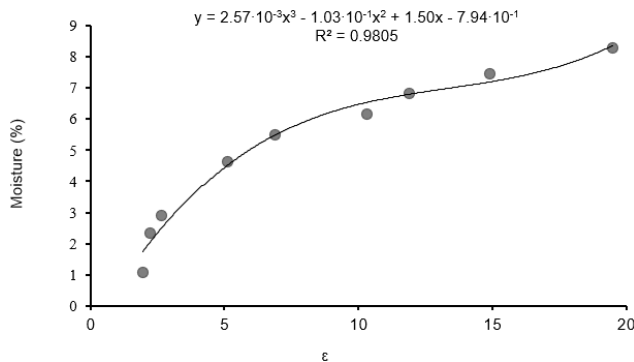
Fig. 9. Natural pellet feed iron ore moisture model.

The drying test was carried out with the wind tunnel at an average speed of 50 km/h, duration of 6 h, and moisture measurements taken every 5 s, that is, a simulation of 300 km on the railroad.

The ore sample prepared for the wind tunnel test had a moisture content of 7.91%, verified by the gravimetric method. Fig. 10 shows the train wagon prototype applied on the wind tunnel: 1) is the train wagon prototype with the capacitive sensor; 2) are the sensor connectors; 3) is the tunnel test section and 4) a hygrometer.

Fig. 10. Wind tunnel test.

Figure 11 shows the result of the wind tunnel test.

$$y = -61.23x^3 + 117.24x^2 - 78.04x + 24.96$$
$$R^2 = 0.9983$$
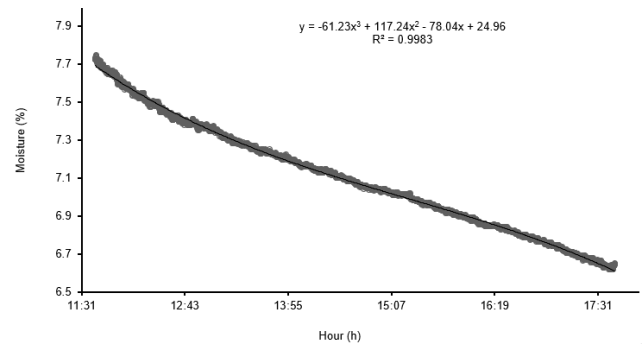
Fig. 11. Drying iron ore behavior on wind tunnel test.

The initial ore moisture measured by the sensor was 7.73% with an error of 0.18 pp compared to the gravimetric method. At the end of the test, the water percentage was 6.60%, so the iron ore presented a drying rate of 1.13 pp.

During the first hour of the test test, we observed a third-order moisture decay. However, after the second hour, a linear moisture decay is observed.

Therefore, the accuracy and the low error observed in the validation process are essential to prove the capacitive sensor efficiency developed. Furthermore, it is an effective measurement instrument to assist in the studies of particulate emissions, and it is an advance to the mining industry that needs to take real-time iron ore measurements.

The research challenge is to scale the sensor to the actual size of a train wagon. Some points still need attention in the future, such as using the side of the wagon as an electrode and studying the behavior of its electric field for real geometry.

IV. CONCLUSION

This work presented the development of a capacitive sensor for real-time moisture measurement, which uses the Real-Dual-Frequency method to determine σ and ε. This approach allows measuring those parameters independently, even for low frequencies, and for conductivity up to 864.4 μS/cm (in this work).

The moisture calibration process, performed using samples up to 13%, achieved high accuracy and a maximum error of 0.39 pp for the 7.49% moisture sample. Thus, the system proved to be quite effective in measuring moisture in an area of great commercial interest (7%-9%).

After proving the sensor's accuracy, it was possible to assist in a wind tunnel test and observe the pellet feed iron ore drying behavior. For a railroad simulation of 300 km to 50 km/h, the drying behavior showed a third-degree curve and a maximum error of 0.18 pp.

Therefore, the real-time iron ore moisture capacitive sensor developed proved suitable for moisture measurement. Moreover, it can be an innovative and crucial resource in the laboratory study of particulate emissions, which objective is to understand the drying behavior of iron ore and other minerals on railways.

ACKNOWLEDGMENT

REFERENCES

[1] "Relatório anual de atividades: Janeiro a dezembro 2021," Instituto Brasileiro de Mineração, Tech. Rep., 2022.

[2] R. S. Jr, A. Fontana, A. Cunha, A. Mesquita, C. Gontijo, and L. L. Filho, "Experimentos em túnel de vento para secagem e emissão de particulados de minério de ferro em modelo de vagões de trem," in *XXVII Encontro Nacional de Tratamento de Minérios e Metalurgia Extrativa*, 2017.

[3] G. Cassini Nazareno, L. Alves da Silva, A. J. de Barros, F. da Fonseca Diniz, and T. E. Drumond Ferreira, "Estudo de caso - poeira nas operações de mina: alta eficiência no controle de particulados a través do uso de supressor natural," *Revista Observatorio de la Economía Latinoamericana*, 2018.

[4] R. M. dos Santos Jr, A. L. A. Mesquita, and M. L. Gemaque, "Development of an open-circuit low-speed wind tunnel," in *23rd ABCM International Congress of Mechanical Engineering*, 2015.

[5] ABNT, *ABNT NBR ISO 3082 - Minério de ferro - Procedimentos de amostragem e preparação de amostras*, ASSOCIAÇÃO BRASILEIRA DE NORMAS TÉCNICAS - ABNT, 2019.

[6] T. B. G. Moreira, "Avaliação de sistemas de drenagem com geossintéticos para diminuição da umidade no minério de ferro da serra de carajás," Master's thesis, Universidade Federal de Minas Gerais, Belo Horizonte, MG, 2011.

[7] E. Pinto, G. Santos, A. R. Segundo, and P. Magalhães, "A novel two degrees of freedom system for measuring iron ore water content on a conveyor belt," *IEEE Sensors Journal*, vol. 21, pp. 16 291 – 16 300, 2021.

[8] T. Saito, T. Oishi, M. Inoue, S. Iida, N. Mihota, A. Yamada, K. Shimizu, S. Inumochi, and K. Inosako, "Low-error soil moisture sensor employing spatial frequency domain transmissometry," *Sensors*, vol. 22, no. 22, p. 8658, 2022.

[9] V. Lage, A. R. Segundo, T. B. e Pinto, C. da Silva, E. Pinto, , and M. Silva, "Bench system for iron ore moisture measurement," in *12th International Conference on Sensing Technology*, 2018, pp. 139–142.

[10] M. Silva, A. R. Segundo, S. da Silva, and P. de Barro Monteiro, "Development of a capacitive, non-invasive and coplanar-electrode transducer for measuring iron ore moisture," in *MDPI Proceedings*, vol. 42, 2019, p. 76.

[11] A. R. Segundo, E. Pinto, G. Santos, and P. B. Monteiro, "Capacitive impedance measurement: Dual-frequency approach," *Sensors*, vol. 19, p. 12, 2019.

[12] A. R. Segundo, G. Santos, E. Pinto, and P. de Barro Monteiro, "Método real-dual-frequency para medição de impedância capacitiva utilizando circuito conversor tensão-corrente," BR Patent 10 2020 005819 3, Mar. 24, 2020, 2020.

[13] E. Pinto, A. R. Segundo, G. Santos, and P. Magalhães, "Sistema de medição de umidade de minério aplicado a um transportador de correia," BR Patent 10 2020 000082 9, 2020, 2020.

[14] R. M. d. SANTOS JUNIOR *et al.*, "Procedimentos experimentais para avaliação da emissão de poeira em manuseio de minério," Master's thesis, Universidade Federal do Pará, 2021.

[15] M. da Silva, "Impedance sensors for fast multiphase flow measurement and imaging," Ph.D. dissertation, Technischen Universität Dresden, 2008.

[16] AGILENT, "Basics of measuring the dielectric properties of materials," 2006.

[17] H.-Y. Chen and C. Chen, "Determination of optimal measurement points for calibration equations—examples by rh sensors," *Sensors*, vol. 21, p. 1213, 2019.

[18] D. A. Robinson, J. P. Bell, , and C. H. Batchelor, "Influence of iron minerals on the determination of soil water content using dielectric techniques," *Journal of Hydrology*, vol. 161, pp. 169–180, 1994.

[19] G. C. Topp and A. P. A. J. L. Davis and, "Electromagnetic determination of soil water content: Measurements in coaxial transmission lines," *Water resources research*, vol. 16, pp. 574–582, 1980.

[20] T. Souza Pinto, A. Souza, J. Batista, A. Sarkis, L. Leal Filho, T. Pádua, and R. Béttega, "Characterization and drying kinetics of iron ore pellet feed and sinter feed," *Drying Technology*, vol. 39, no. 10, pp. 1359–1370, 2021.

Gabriel A. Santos received the B.Sc. degree in Electrical Engineering from the Instituto Federal de Educação, Ciência e Tecnologia da Bahia (IFBA), Brazil, in 2017, and the M.Sc. degree in Instrumentation, Control, and Automation of Mining Process from the Universidade Federal de Ouro Preto (UFOP) and the Instituto Tecnológico Vale (ITV), Ouro Preto, Brazil, in 2020.

Érica S. Pinto received the B.Sc. degree in Control and Automation Engineering from the Universidade Federal de Ouro Preto (UFOP), Ouro Preto, Brazil, in 2017, and the M.Sc. degree in Instrumentation, Control, and Automation of Mining Process from UFOP and the Instituto Tecnológico Vale, Ouro Preto, Brazil. She is currently a D.Sc. student in computer science at UFOP.

Artur J. C. da Silva received the B.Sc. degree in Mechanical Engineering from the Universidade Federal do Pará (UFPA), Brazil in 2019 and the M.Sc. degree in Infrastructure and Energy Development from the Universidade Federal do Pará (UFPA), Brazil in 2022. He is currently a professor of metal mechanics at the Serviço Nacional de Aprendizagem Industrial (SENAI) in Canaã dos Carajás, Brazil.

Paulo M. de B. Monteiro received the B.Sc. degree in Electronic and Telecommunications Engineering from the Pontifícia Universidade Católica de Minas Gerais in 1978, a master's degree in Mechanical Engineering from the Universidade Federal de Uberlândia in 1994, and a Ph.D. in Agricultural Engineering from the Universidade Federal de Viçosa in 2002. He is currently a collaborating professor at the Universidade Federal de Viçosa and a full professor at the Universidade Federal de Ouro Preto (UFOP).

André L. A. Mesquita received the B.Sc. degree in Mechanical Engineering from the Universidade Federal do Pará (UFPA) in 1984, Brazil, a Master's degree in Aeronautical and Mechanical Engineering from the Instituto Tecnológico de Aeronáutica (ITA) in 1987, Brazil and a PhD in Mechanical Engineering from the Institut National Polytechnique in 1992, Grenoble, France. He is currently a professor at the Universidade Federal do Pará (UFPA) and Director of TECNOLAGO - Technology Park of Lago in Tucuruí Brazil.

Alan Kardek R. Segundo received the B.Sc. degree in Control and Automation Engineering from the Universidade Federal de Ouro Preto (UFOP), Ouro Preto, Brazil, in 2008, and the M.Sc. and D.Sc. degrees in Agricultural Engineering from the Universidade Federal de Viçosa, Viçosa, Brazil, in 2010, and 2014, respectively. He is currently a Reseacher with the Universidade Federal de Ouro Preto and the Instituto Tecnológico Vale, Ouro Preto, Brazil.